2D Materials

RECEIVED
1 August 2016

REVISED
29 September 2016

ACCEPTED FOR PUBLICATION
14 October 2016

PUBLISHED
26 October 2016

PAPER

Highly efficient, high speed vertical photodiodes based on few-layer MoS_2

Zhen Li[1,4], **Jihan Chen**[1,4], **Rohan Dhall**[1] **and Stephen B Cronin**[1,2,3]

[1] Departments of and Electrical Engineering, University of Southern California, Los Angeles, CA 90089, USA
[2] Physics and Astronomy, University of Southern California, Los Angeles, CA 90089, USA
[3] Chemistry, University of Southern California, Los Angeles, CA 90089, USA
[4] These authors contributed equally.

E-mail: scronin@usc.edu

Keywords: transition metal dichalcogenide, MoS_2, photodetector, vertical device

Supplementary material for this article is available online

Abstract

Layered transition metal dichalcogenides, such as MoS_2, have recently emerged as a promising material system for electronic and optoelectronic applications. The two-dimensional nature of these materials enables facile integration for vertical device design with novel properties. Here, we report highly efficient photocurrent generation from vertical MoS_2 devices fabricated using asymmetric metal contacts, exhibiting an external quantum efficiency of up to 7%. Compared to in-plane MoS_2 devices, the vertical design of these devices has a much larger junction area, which is essential for achieving highly efficient photovoltaic devices. Photocurrent and photovoltage spectra are measured over the photon energy range from 1.25 to 2.5 eV, covering both the 1.8 eV direct K-point optical transition and the 1.3 eV Σ-point indirect transition in MoS_2. Photocurrent peaks corresponding to both direct and indirect transitions are observed in the photocurrent spectra and exhibit different photovoltage–current characteristics. Compared to previous in-plane devices, a substantially shorter photoresponse time of 7.3 μs is achieved due to fast carrier sweeping in the vertical devices, which exhibit a −3 dB cutoff frequency of 48 kHz.

2D layered materials, including graphene, transition metal dichalcogenides (TMDCs), and black phosphorous, have attracted great research interest in the past decade. Unlike graphene, TMDCs such as MoS_2 exhibit finite bandgaps in the visible wavelength range [1–4]. Furthermore, the band structures of MoS_2 and other TMDCs depend on the number of layers of material [1]. While most research on MoS_2 has focused on the indirect-to-direct band gap transition occurring in monolayer MoS_2, this has an inherently small optical density that limits its potential application in practical optoelectronic devices. Few-layer MoS_2 films, on the other hand, provide substantially larger optical densities than monolayers and can withstand substantially higher injection currents, which are advantageous for solar energy conversion and light emitting diode applications. Various MoS_2 devices have been fabricated and studied to improve the performance of MoS_2, including graphene/MoS_2 [5], monolayer TMDC stacks [6–8], and MoS_2/metal junctions [9–11]. Because of the absence of dangling bonds at the interfaces of two-dimensional materials, the Schottky junction between metals and MoS_2 more 'ideal' than 3D semiconductors like Si or III–V compounds [12, 13]. This is an essential advantage of TMDCs, which enables the possibility of building vertical MoS_2 devices with atomically clean and sharp interfaces, leading to unique physics, such as split excitons [14], interlayer charge transfer [7], and plasmonic-exciton interactions [9–11].

In previous studies of in-plane MoS_2 photodetectors [15–18], the charge separation region of the device is defined by the Schottky junction between the metal and the MoS_2. As a result, only incident light shining within the depletion width, which is only approximately 100 nm, can generate a photocurrent. To improve this, comb-shaped source and drain metal electrodes have been introduced to increase the effective charge separation region [18]. Nevertheless, the effective area is still a small fraction (less than 1%) of

the device footprint. In addition, the efficiency of monolayer in-plane devices is further limited by the small optical density of monolayer MoS_2. Lastly, a gate bias and large drain-source bias voltages (10 V) are essential for obtaining high sensitivity in these in-plane devices, which gives rise to high power consumption and may eventually degrade the device [19].

In the work presented here, we use few-layer instead of monolayer MoS_2, with a vertical device structure. By utilizing few-layer MoS_2 in a cross-plane geometry, the optical density is enhanced and the effective charge separation region is increased to the entire volume of the MoS_2 flake. As a result, an external quantum efficiency (EQE) of up to 7% is achieved, which is more than 100 times larger than previous reports based on monolayer MoS_2 flakes [20]. Also, the trapped charge and surface states in the in-plane devices result in large time delays, which limit the cutoff frequency to less than 200 Hz [16]. In the vertical few-layer devices presented here, the TMDC is insulated from moisture and other kinds of dopants in air by the top electrode. This reduces the delay time because there is a smaller amount of surface charge and unintentional dopants. Also, the shorter channel lengths in the vertical devices make it easier for the remaining carriers to be collected by the electrodes when the light is off, further reducing the response time of the device. A substantially lower delay is obtained using the AC lock-in technique, which exhibits a -3 dB cutoff frequency of 48 kHz, corresponding to time response of 7.3 μs ($t_r = 0.35/f_{\text{cut-off}}$).

The devices measured in this work are fabricated using a dry transfer technique, as shown in figures 1(a) and (b) [21]. First, the MoS_2 flake is exfoliated onto a piece of PDMS mounted on a glass slide. Target MoS_2 flakes are identified using an optical microscope. The MoS_2 flake is then transferred from the PDMS stamp onto a Si/SiO_2 (300 nm) substrate with pre-patterned metal electrodes (1 nm/30 nm Ti/Au) using a home built contact aligner. After the transfer, a semi-transparent 10 nm Pd film is deposited as the top electrode. After fabrication, photoluminescence (PL) spectra are measured from the few-layer flake, as shown in figure 1(c). In addition to the PL peaks at 1.8 eV and 2.0 eV corresponding to the direct band transitions at the K-point of the Brillouin zone [1, 2], there is another weaker peak around 1.3 eV, which corresponds to the indirect transition at the Σ-point. In this fabrication scheme, different metals (with different work functions) are used for the top and bottom electrodes of the MoS_2 flake. Au is used for the bottom electrode while top electrode is Pd. According to previous studies on graphene and MoS_2 [22, 23], an asymmetric contact for the source and drain will break the mirror symmetry of the internal electric fields in the channel, and improve the photovoltaic performance of the device. Given that the work function of Pd is 5.6 eV, and the electron affinity of MoS_2 is about 4.4 eV [24], the Pd serves as a hole-doping contact for MoS_2. On the other hand, Au is electron-doping, so the two Schottky junctions formed at these contacts produce an additive photovoltaic effect [5, 23]. Based on the optical properties of Pd films in the visible range [25, 26], the absorption coefficient of Pd at visible range is about 50–80 μm^{-1}. As a result, only about 50% of the incident illumination will penetrate the 10 nm Pd top electrode film. We expect there to be a tradeoff between optical density (which increases with thickness) and series conductance (which decreases with thickness). Another constraint here is that the thickness of the top Pd electrode must be thicker than the MoS_2 flake in order to be provide a continuous electrode at the step edge (i.e., boundary) of the MoS_2 flake. This means that if we further increase the thickness of the MoS_2 flake, we need to deposit a thicker top metal electrode, which will very quickly become opaque. In general, MoS_2 flakes around 10 nm are best for our device structures. Figure 2(a) shows photocurrent spectra measured from the few-layer MoS_2 vertical device. As in the PL spectra shown in figure 1(c), the dominant photocurrent peaks start around 1.8 eV and extend to 2.2 eV, corresponding to the direct transitions at the K-point in the Brillouin zone. Interestingly, a few lower energy peaks are observed around 1.2–1.4 eV, likely due to indirect transitions at the Σ-point, which have not been reported previously. The power spectrum of the incident laser light is plotted in figure 2(b). Given an effective illumination of 50%, considering the light absorption in the top Pd electrode, the EQE is calculated and plotted together with the power spectrum in figure 2(b). As a comparison, previous photocurrent spectra measured from monolayer MoS_2 exhibited EQEs of about 2.5×10^{-4} [20], mainly due to low optical density of the monolayer and also the small area of the in-plane charge separation region. From the vertical few-layer MoS_2 device with asymmetric metal contacts, an EQE of up to 7% is achieved. In addition to the short circuit current, we also measured the open circuit voltage from the device, as plotted in figure 2(c). The open circuit voltage of the device is relatively small, less than 80 mV. It is know that a Schottky photodiode usually suffers from low output voltage, because of the large dark saturation current [27, 28]. In a pn-junction photodiode, the open circuit voltage obeys the following relation:

$$V_{oc} = \frac{kT}{q} \ln\left(1 + \frac{I_{sc}}{I_o}\right) \approx \frac{kT}{q} \ln \frac{I_{sc}}{I_o},$$

where I_{sc} is the short circuit current, I_o is the dark saturation current, and $I_o \ll I_{sc}$. In our vertical MoS_2 device, the thickness of the few-layer MoS_2 is only 10 nm (see figure S1), which is well below the depletion width of the corresponding bulk semiconductor device. In this case, the leakage current caused by the drift of photoexcited carriers is not a constant, but related to the incident photon number. As a result, the tunneling effect makes this device very leaky, and the

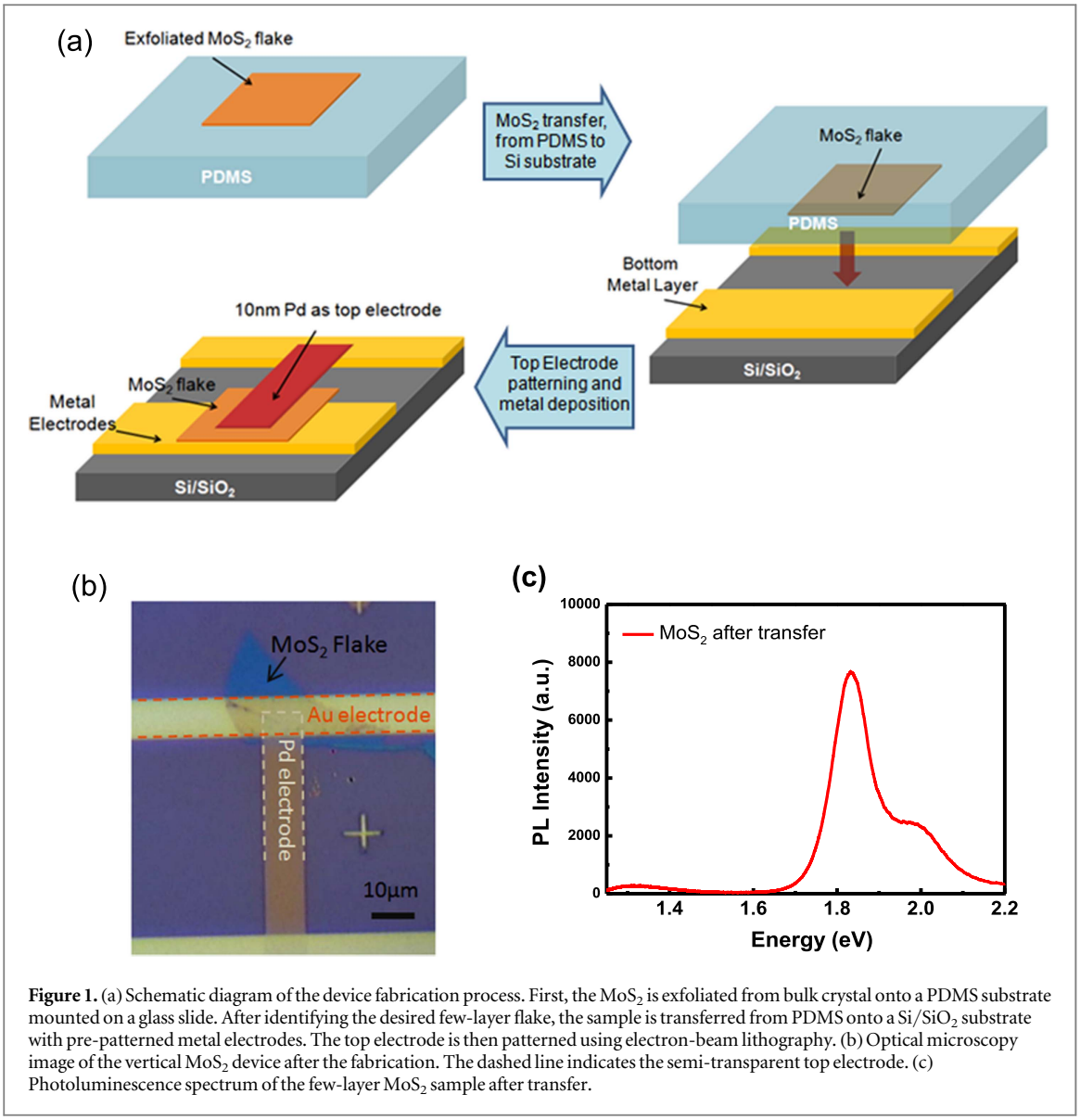

Figure 1. (a) Schematic diagram of the device fabrication process. First, the MoS_2 is exfoliated from bulk crystal onto a PDMS substrate mounted on a glass slide. After identifying the desired few-layer flake, the sample is transferred from PDMS onto a Si/SiO_2 substrate with pre-patterned metal electrodes. The top electrode is then patterned using electron-beam lithography. (b) Optical microscopy image of the vertical MoS_2 device after the fabrication. The dashed line indicates the semi-transparent top electrode. (c) Photoluminescence spectrum of the few-layer MoS_2 sample after transfer.

V_{oc} is small , only a few kT. The V_{oc}–I_{sc} relation is plotted in figure 2(d). Instead of a logarithmic relationship, the V_{oc}–I_{sc} relation is rather linear. Also, we observe two distinct behaviors in the relation between V_{oc} and I_{sc}, which varies with different incident photon energy. The data points associated with incident photon energies between 1.75 and 2.25 eV (K-point transition) have a different slope than those obtained with photon energies between 1.25 and 1.4 eV (Σ-point transition). This difference can be explained by considering the different band gap energies of these two optical transitions. Since the band gap at the K-point is approximately 0.5 eV higher than the Σ-point band gap, we expect the open circuit voltage to be higher in the case of the K-point excitation. Lastly, we estimate the electrical output power and energy conversion efficiency of the device (see figure 2(e)) based on both the short circuit current and the open circuit voltage, and by assuming a fill factor of 0.25. With 7 μW total incident optical power, 4 nW of electrical power can be extracted from the device. It is not surprising that the energy conversion efficiency of the device is relatively low due to the small thickness of the device and a large leakage current.

As we mentioned above, the thickness of few-layer MoS_2 is much smaller than the 'depletion width' and the minority carrier diffusion length. Because of this, the I–V characteristics measured from this device are exhibit a linear dependence, as shown in figure 3, instead of rectifying behavior. This linear behavior also limits the energy conversion efficiency of the device by restricting the fill factor to just 0.25. Figure 3 shows the photo-I–V characteristics of a device under different incident laser powers (532 nm wavelength, power 0.92, 12, and 108 μW). With higher incident optical powers, the I_{sc} is increased from 1.3 to 400 nA, and V_{oc} is increased from 1 to 100 mV.

Compared to an in-plane MoS_2 device, the very short 'channel length' of the vertical device, which is smaller than the depletion width, limits the device's performance as a diode. On the other hand, the short channel length also increased the conductance of these vertical few-layer devices by more than 1000 times,

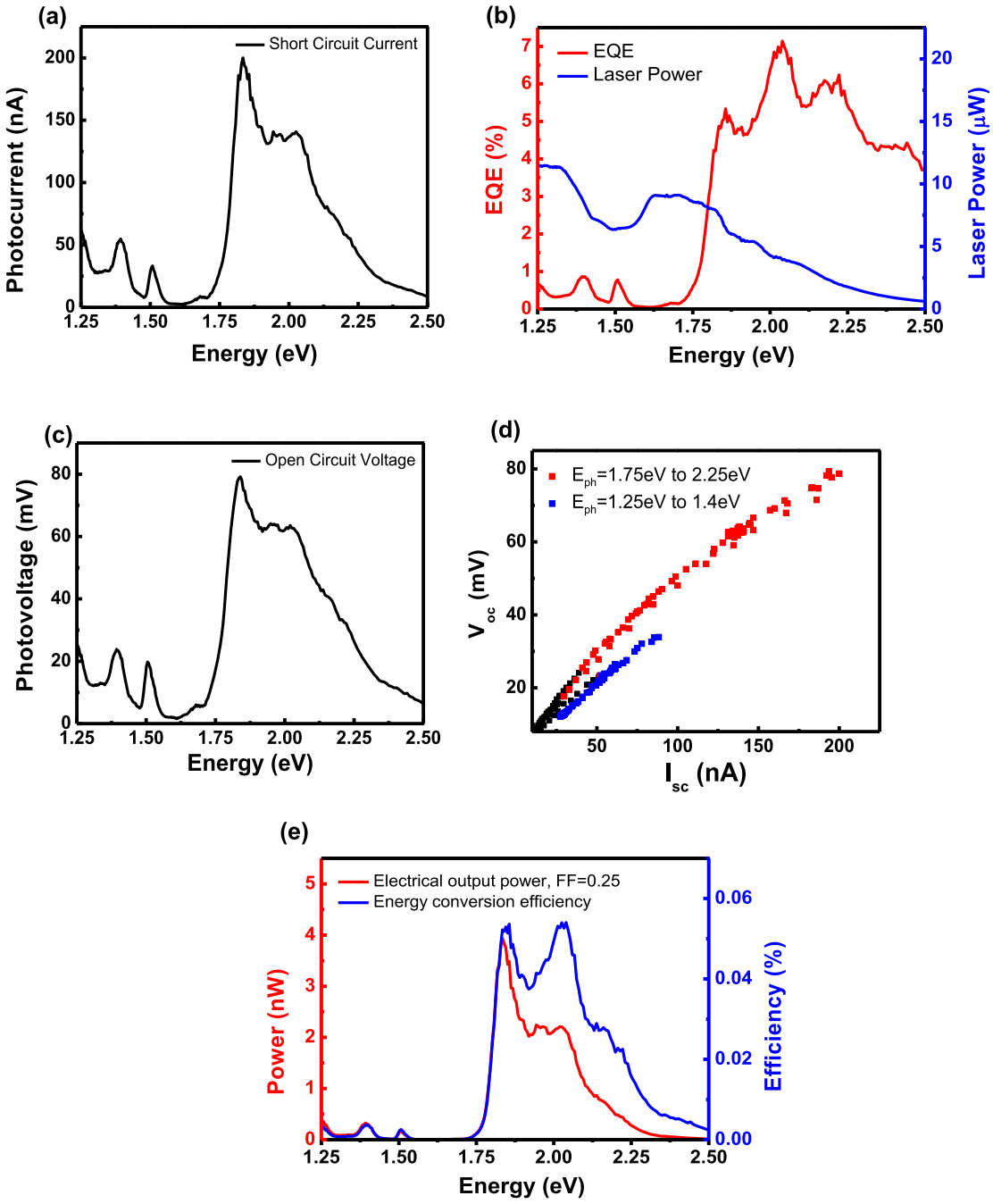

Figure 2. (a) Photocurrent and (c) photovoltage spectra of the vertical MoS_2 device. In addition to the main peak around 1.8–2.1 eV, lower energy peaks at 1.4 and 1.5 eV are also observed due to the indirect transition. (b) Power spectrum of the incident laser plotted together with the EQE of the device. The two peaks at 1.85 and 2.0 eV correspond to the K-point transition. The EQE of the direct transition is about 10 times larger than the indirect transition. (d) I_{sc}–V_{oc} plot showing that the direct band transition (red points) and the indirect band transition (blue points) give different I_{sc}–V_{oc} relations. (e) Extracted electrical power and energy conversion efficiency estimated from the product of the short circuit current and open circuit voltage, assuming a fill factor of 0.25.

compared to in-plane MoS_2 photodetectors [16–18]. As such, our vertical device can operate at a lower voltage and does not require the application of an externally applied gate voltage, both of which reduce the power consumption significantly A photoresponsivity of 10 mA W^{-1} is measured at a bias voltage of 0.1 V (under an optical power density of 1 μW μm^{-2}), which is more than 10X larger than the maximum value measured from an in-plane MoS_2 device under the same bias voltage [15, 18].

The very short channel length and built-in electric field in the depletion region help eliminate the photon generated carriers and trapped charges when the illumination is off. This makes the vertical device response much faster than a corresponding in-plane device. The time-resolved photoresponse of the device is shown in figure 4(a). Here, a 680 nm diode laser (Communications Grade VCSEL) is used as the light source, modulated by a function generator (Agilent EE4432B) at 1 kHz. The output open circuit

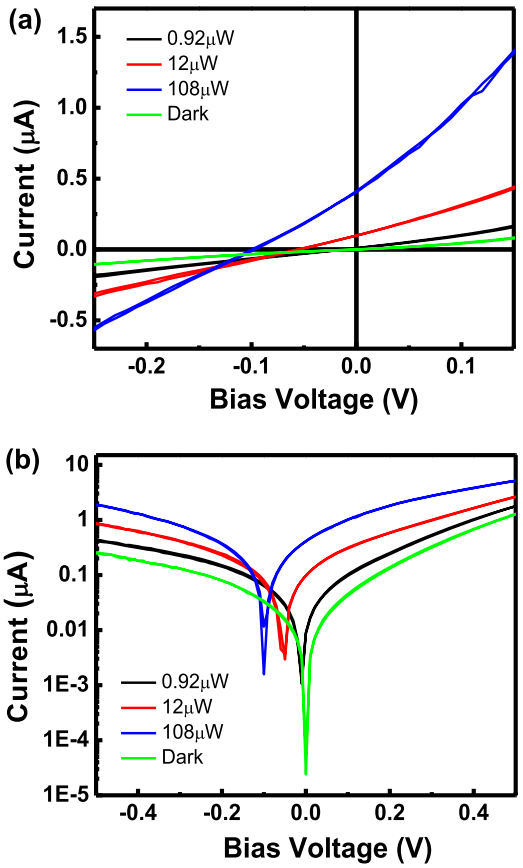

Figure 3. (a) Photo-*I*–*V* characteristics of the vertical MoS_2 device under 532 nm illumination. (b) Log plot of the photo-*I*–*V* data.

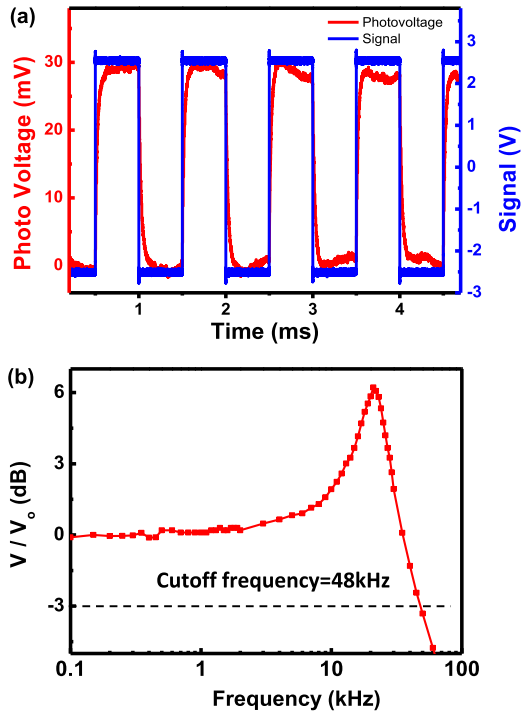

Figure 4. (a) Photovoltage plotted as a function of time under modulated 680 nm laser illumination. The photovoltage signal is processed after FFT filtering to remove high frequency noise, with the cutoff frequency of the FFT filtering set to 100 kHz. (b) The frequency response of the open circuit photovoltage, which shows a cutoff frequency at 48 kHz. V_o is the photovoltage measured with continuous light illumination.

photovoltage and its rise and fall time are measured using an oscilloscope (Agilent Infiniium MSO8104A), as plotted in figure 4(a). To further investigate the frequency response of the vertical MoS_2 device, an AC measurement is performed using a lock-in amplifier. The frequency of the light modulation is varied from 100 Hz to 100 kHz, which shows a cutoff frequency of 48 kHz, showing figure 4(b). The peak in the frequency response of this device around 20 kHz is related to the RLC resonance of the circuit, as described in more detail in the Supplemental Document. Here, our device is operated without any applied gate or bias voltage, and exhibits an open circuit voltage cutoff frequency of 48 kHz. The cutoff frequency measured from the lock-in shows that the response time of our device is 7.3 μs, which is over 10 times faster than the best result from corresponding in-plane device [16, 18].

Conclusion

In summary, we have shown that vertical metal/MoS_2/metal devices with asymmetric metal contacts can be used for highly efficient photocurrent generation and photodetection, with an EQE of up to 7%. in contrast to typical values of in-plane devices which span a wide range from 0.02% to 0.1% under the same illumination power density [20, 29]. For the first time, the photocurrent spectra are measured from a few-layer MoS_2 device exhibiting lower energy photocurrent peaks around 1.2–1.4 eV, corresponding to the Σ-point indirect transition. A photoresponsivity of 10 mA W^{-1} is measured at a bias voltage of 0.1 V. The vertical device can be run at zero bias voltage without any gating, which reduces the power consumption significantly compared to the corresponding in-plane MoS_2 devices. Also, we performed the first frequency response measurement on vertical MoS_2 photodetectors, which show a bandwidth of 48 kHz. The cutoff frequency may be further increased by optimizing the device design to reduce the parasitic capacitance. The *I*–*V* characteristics of the device show a linear behavior because the thickness of the few-layer MoS_2 is smaller than the 'depletion width' and the minority carrier diffusion length. Increasing the thickness of the MoS_2 flakes will reduce the leakage current and result in more rectifying behavior. The metal/MoS_2/metal vertical structure presents a more effective design layout with a larger photovoltaic area than corresponding in-plane devices, and can readily be integrated with silicon microelectronics.

Methods

Fabrication of vertical few-layer MoS_2 device

Few-layer MoS_2 films were exfoliated from bulk MoS_2 (SPI Supplies) onto PDMS based gel (Gel-Pack®, #PF-3-X4) mounted on a glass slide with pre-patterned alignment markers using the 'Scotch tape' method [30]. After identifying the target MoS_2 flake, the glass slide with the film is then mounted in a X–Y–Z micromanipulator. With the alignment markers on the glass slide, the MoS_2 can be readily located using an optical microscope and then the transferred onto a Si/SiO_2 (300 nm) substrate with pre-patterned metal electrodes (1 nm Ti and 30 nm gold), as illustrated in figure 1(a). The top electrode is fabricated using electron-beam lithography followed by 10 nm Pd deposition, as shown in figure 1(b).

Photoluminescence spectroscopy and photo-*I–V* measurement

Photoluminescence spectra and photo-*I–V* characteristics are taken using a Renishaw *InVia* spectrometer with a 532 nm laser focused through a 100× objective lens. PL spectra are collected at room temperature, under ambient conditions. The *I–V* characteristics are recorded using an HP 4145B semiconductor parameter analyzer.

Photocurrent and photovoltage spectra

Photocurrent spectra are collected using a Fianium supercontinuum white light laser source in conjunction with a Princeton Instruments double grating monochromator to provide monochromatic light over the 450–1000 nm wavelength range. A Keithley 2401 SourceMeter® is used for the electrical measurement. The laser power is measured using a ThorLabs PM100D power and energy meter.

Time response measurement and frequency response measurement

A 680 nm diode laser (Communications Grade VCSEL) is used for the measurement. The turn on voltage of the diode laser is 2.2 V. A function generator (Agilent EE4432B) is used as the power supply of the diode laser. The output signal of the function generator is set as a 1 kHz square wave. The output photovoltage is measured using an oscilloscope (Agilent Infiniium MSO8104A). In the frequency response measurement, a lock-in amplifier (Stanford Research Systems, SR830) is used as the voltage supply for the diode laser, while the frequency is swept from 100 Hz to 100 kHz.

Acknowledgments

This research was supported by Department of Energy (DOE) Award No. DE-FG02–07ER46376 (ZL) and NSF Award No. 1402906 (JC).

Reference

[1] Mak K F, Lee C, Hone J, Shan J and Heinz T F 2010 Atomically thin MoS_2: a new direct-gap semiconductor *Phys. Rev. Lett.* **105** 4
[2] Splendiani A, Sun L, Zhang Y, Li T, Kim J, Chim C-Y, Galli G and Wang F 2010 Emerging photoluminescence in monolayer MoS_2 *Nano Lett.* **10** 1271–5
[3] Wang Q H, Kalantar-Zadeh K, Kis A, Coleman J N and Strano M S 2012 Electronics and optoelectronics of two-dimensional transition metal dichalcogenides *Nat. Nanotechnol.* **7** 699–712
[4] Chhowalla M, Shin H S, Eda G, Li L-J, Loh K P and Zhang H 2013 The chemistry of two-dimensional layered transition metal dichalcogenide nanosheets *Nat. Chem.* **5** 263–75
[5] Yu W J, Liu Y, Zhou H, Yin A, Li Z, Huang Y and Duan X 2013 Highly efficient gate-tunable photocurrent generation in vertical heterostructures of layered materials *Nat. Nanotechnol.* **8** 952–8
[6] Gong Y, Lin J, Wang X, Shi G, Lei S, Lin Z, Zou X, Ye G, Vajtai R and Yakobson B I 2014 Vertical and in-plane heterostructures from WS_2/MoS_2 monolayers *Nat. Mater.* **13** 1135–42
[7] Lee C-H *et al* 2014 Atomically thin p–n junctions with van der Waals heterointerfaces *Nat. Nanotechnol.* **9** 676–81
[8] Dhall R, Neupane M R, Wickramaratne D, Mecklenburg M, Li Z, Moore C, Lake R K and Cronin S 2015 Direct bandgap transition in many-layer MoS_2 by plasma-induced layer decoupling *Adv. Mater. (Weinheim, Germany)* **27** 1573
[9] Buscema M, Steele G A, van der Zant H S and Castellanos-Gomez A 2014 The effect of the substrate on the Raman and photoluminescence emission of single-layer MoS_2 *Nano Res.* **7** 1–11
[10] Bhanu U, Islam M R, Tetard L and Khondaker S I 2014 Photoluminescence quenching in gold–MoS_2 hybrid nanoflakes *Sci. Rep.* **4** 5575
[11] Li Z, Ezhilarasu G, Chatzakis I, Dhall R, Chen C-C and Cronin S B 2015 Indirect band gap emission by hot electron injection in metal/MoS_2 and metal/WSe_2 heterojunctions *Nano Lett.* **15** 3977–82
[12] Tung R T 2000 Chemical bonding and Fermi level pinning at metal-semiconductor interfaces *Phys. Rev. Lett.* **84** 6078
[13] Lince J R, Carré D J and Fleischauer P D 1987 Schottky-barrier formation on a covalent semiconductor without Fermi-level pinning: the metal–MoS_2(0001) interface *Phys. Rev.* B **36** 1647–56
[14] Huang C, Wu S, Sanchez A M, Peters J J, Beanland R, Ross J S, Rivera P, Yao W, Cobden D H and Xu X 2014 Lateral heterojunctions within monolayer $MoSe_2$–WSe_2 semiconductors *Nat. Mater.* **13** 1096–101
[15] Yin Z, Li H, Li H, Jiang L, Shi Y, Sun Y, Lu G, Zhang Q, Chen X and Zhang H 2011 Single-layer MoS_2 phototransistors *ACS Nano* **6** 74–80
[16] Lopez-Sanchez O, Lembke D, Kayci M, Radenovic A and Kis A 2013 Ultrasensitive photodetectors based on monolayer MoS_2 *Nat. Nanotechnol.* **8** 497–501
[17] Choi W, Cho M Y, Konar A, Lee J H, Cha G B, Hong S C, Kim S, Kim J, Jena D and Joo J 2012 High-detectivity multilayer MoS_2 phototransistors with spectral response from ultraviolet to infrared *Adv. Mater.* **24** 5832–6
[18] Tsai D-S, Liu K-K, Lien D-H, Tsai M-L, Kang C-F, Lin C-A, Li L-J and He J-H 2013 Few-layer MoS_2 with high broadband photogain and fast optical switching for use in harsh environments *ACS Nano* **7** 3905–11
[19] Ionescu A M and Riel H 2011 Tunnel field-effect transistors as energy-efficient electronic switches *Nature* **479** 329–37
[20] Li Z, Chang S-W, Chen C-C and Cronin S B 2014 Enhanced photocurrent and photoluminescence spectra in MoS2 under ionic liquid gating *Nano Res.* **7** 973–80
[21] Castellanos-Gomez A, Buscema M, Molenaar R, Singh V, Janssen L, van der Zant H S and Steele G A 2014 Deterministic transfer of two-dimensional materials by all-dry viscoelastic stamping *2D Materials* **1** 011002

[22] Mueller T, Xia F and Avouris P 2010 Graphene photodetectors for high-speed optical communications *Nat. Photon.* **4** 297–301
[23] Fontana M, Deppe T, Boyd A K, Rinzan M, Liu A Y, Paranjape M and Barbara P 2013 Electron–hole transport and photovoltaic effect in gated MoS_2 Schottky junctions *Sci. Rep.* **3** 1634
[24] Schlaf R, Lang O, Pettenkofer C and Jaegermann W 1999 Band lineup of layered semiconductor heterointerfaces prepared by van der Waals epitaxy: charge transfer correction term for the electron affinity rule *J. Appl. Phys.* **85** 2732–53
[25] Sullivan B T 1990 Optical properties of palladium in the visible and near UV spectral regions *Appl. Opt.* **29** 1964–70
[26] Heavens O S 1955 *Optical Properties of Thin Solid Films* (New York: Academic)
[27] Peckerar M, Lin H and Kocher R 1975 Open circuit voltage of MIS Schottky diode solar cells *1975 Int. IEEE Electron Devices Meeting* pp 213–6
[28] Ponpon J and Siffert P 1976 Open-circuit voltage of MIS silicon solar cells *J. Appl. Phys.* **47** 3248–51
[29] Zhang W, Chuu C-P, Huang J-K, Chen C-H, Tsai M-L, Chang Y-H, Liang C-T, Chen Y-Z, Chueh Y-L and He J-H 2014 Ultrahigh-gain photodetectors based on atomically thin graphene-MoS_2 heterostructures *Sci. Rep.* **4** 3826
[30] Novoselov K S, Geim A K, Morozov S, Jiang D, Zhang Y, Dubonos S A, Grigorieva I and Firsov A 2004 Electric field effect in atomically thin carbon films *Science (Washington, DC)* **306** 666–9